Available online at www.sciencedirect.com
SCIENCE DIRECT®
Journal of Molecular Catalysis A: Chemical 229 (2005) 233–239
JOURNAL OF MOLECULAR CATALYSIS A: CHEMICAL
www.elsevier.com/locate/molcata

Gas-phase photo-oxidations of organic compounds over different forms of zirconia

Chunying Wu, Xiping Zhao, Yingjie Ren, Yinghong Yue*, Weiming Hua, Yong Cao, Yi Tang, Zi Gao

Department of Chemistry and Shanghai Key Laboratory of Molecular Catalysis and Innovative Materials, Fudan University, Shanghai 200433, PR China

Received 9 November 2004; received in revised form 29 November 2004; accepted 29 November 2004

Abstract

Nanosized zirconia powders with different phase structure and specific surface area were prepared by various methods and were used as catalysts for gas-phase photocatalytic oxidations of methanol and hexane. The phase structure of the samples was analyzed by X-ray diffraction and Raman spectroscopy. The photocatalytic activity of the amorphous zirconia synthesized in this experiment is much higher than that of the crystalline samples. The activity of hexane oxidation on ZrO_2-0-110 reaches 25.6%, which is even higher than that of Degussa P25 (17.3%). Thermal gravimetric studies show that the high activity is due to the abundant surface hydroxyl groups on the catalysts. Sulfation of zirconia samples induces a decrease in the amount of surface hydroxyl groups and has a negative influence on the activity of the zirconia photocatalysts. The results of a 100 h test show that the activity of the synthesized amorphous zirconia catalyst is very stable.

Keywords: Nanosized zirconia; Photocatalytic oxidation; Amorphous; Crystalline; Surface hydroxyl group; Sulfation

1. Introduction

In the past decade, the significance of semiconductor photocatalysis as a potential environmental control technology has aroused tremendous interest in semiconductor photochemistry and photophysics [1]. Many oxide and sulfide semiconductors such as TiO_2, WO_3, ZnO, $SrTiO_3$, ZnS and CdS are found to exhibit photocatalytic activity for a wide range of chemical reactions. Among the metal oxides, ZrO_2 has been considered recently as a photocatalyst in photochemical heterogeneous reactions due to its relatively wide E_g value and the high negative value of the conduction band potential [2–4]. The reported values of the energy of the band gap energy of this oxide range between 3.25 and 5.1 eV, depending on the preparation technique of the sample, and the most frequent and accepted value is 5.0 eV, with a conduction band potential of −1.0 V versus NHE at pH 0 [3,4]. Previous literature [2–7] reported the application of zirconia photocatalyst for several reactions, including H_2 evolution from water, oxidation of 2-propanol to acetone, oxidation of propene and ethane, photodegradation of 4-chlorophenol, 4-nitrophenol and 1,4-pentanediol, oxidation of CO, photoreduction of aqueous carbonate, oxygen isotopic exchange, and reduction of CO_2 with H_2.

The activity of the photocatalyst is influenced by its crystallinity as well as other factors such as surface area, crystal size, synthesis method, band gap, porosity, crystal phase, and surface acidity. On the basis of extensive studies on the photocatalysis of TiO_2, high crystallinity reduces defective sites of the catalyst, decreases the probability of e^-–h^+ recombination, and hence shows high activity. However, Kominami et al. [8] found that amorphous Nb_2O_5 samples prepared by the solvothermal method exhibited much higher activity than that of the crystalline Nb_2O_5 samples for the photocatalytic

* Corresponding author. Tel.: +86 21 65642409; fax: +86 21 65641740.
E-mail address: yhyue@fudan.edu.cn (Y. Yue).

1381-1169/$ – see front matter © 2004 Elsevier B.V. All rights reserved.
doi:10.1016/j.molcata.2004.11.029

dehydrogenation of methanol and the photocatalytic mineralization of acetic acid in aqueous solutions.

In this work, nanosized zirconia samples were prepared by different methods and characterized by XRD, TG/DTA, UV–vis spectra and N_2 adsorption method. The gas-phase photocatalytic oxidations of methanol and hexane on the zirconia catalysts were studied and correlated to the phase structure, specific surface area and the surface property of the catalysts. The influence of sulfation on the photocatalytic activity of the catalysts was investigated as well.

2. Experimental

2.1. Catalyst preparation

The zirconia precursors were synthesized by a precipitation method [9]. The 6.0 mol l^{-1} aqueous NH_3 solution was added dropwise to 0.4 mol l^{-1} $ZrOCl_2$ solution under stirring until pH 10.0, and then aged at 0 °C for 24 h. The obtained white precipitate was filtered, washed thoroughly with deionized water, dried at 110 °C for 24 h, ground into a fine powder and labeled as ZrO_2-0-110. To obtain the amorphous and tetragonal ZrO_2 catalysts, the zirconia precursor was calcined at different temperatures for 3 h. These catalysts were labeled as ZrO_2-0-110-t, where t stood for the calcination temperature.

The monoclinic ZrO_2 catalyst was prepared by the hydrolysis of Zr-alkoxide [10]. In a typical synthesis, 0.0223 mol of zirconium propoxide ($Zr(OC_3H_7)_4$) was first dissolved in 50 ml of 1-propanol and the solution was slowly poured into 300 ml distilled water with vigorous stirring at room temperature. The mixed solution was allowed to continue stirring for 1 h. The precipitate obtained was filtered, washed with distilled water and dried at 110 °C for 24 h, and then was calcined in air at 650 °C for 3 h. The obtained product was labeled as ZrO_2-110-650.

Sulfated zirconia catalysts were prepared by immersing uncalcined zirconia precursors (ZrO_2-0-110) in 1 mol l^{-1} H_2SO_4 for 45 min, followed by filtering, drying at 110 °C and calcining at 650 °C for 3 h. The samples before and after calcination were labeled as ZrO_2-0-110/SO_4^{2-}-110 and ZrO_2-0-110/SO_4^{2-}-650, respectively.

2.2. Characterization

The crystalline phases of the zirconia catalysts were characterized by X-ray powder diffraction (XRD). A Siemens D8 Advanced X-ray diffractometer with a Cu Kα radiation, a scan speed of 8° min^{-1} and a scan range of 20–70° was used. The surface areas of the catalysts were measured by nitrogen adsorption at 77 K using a Micromeritics ASAP 2000 instrument and calculated by BET method. The morphologies of representative zirconia catalysts were examined by transmission electron microscopy (TEM) using a JEOL-2011 instrument. Thermogravimetric analysis (TG/DTA/DTG) was performed on a Rigaku Thermoflex System with a temperature ramp rate of 10 °C min^{-1} in flowing N_2 and the amount of sample used was 30 mg. Raman spectra was obtained using a confocal microprobe Raman system (Lab Ram Infinity). The excitation wavelength was 514.5 nm from an internal argon ion laser with a power of 8 mW. UV–vis diffuse reflectance spectra were obtained with a JASCO-V-550 UV-Vis spectrometer.

2.3. Photocatalytic oxidations of hexane and methanol

The photocatalytic oxidation of hexane was carried out in a continuous fix-bed flow microreactor under atmospheric pressure. The 0.3 g (20–40 mesh) catalyst was pretreated in flowing N_2 for 0.5 h. Hexane (1700 ppm) and balance air with a space velocity (GHSV) of 4000 h^{-1} were passed through the catalyst overnight to reach adsorption equilibrium, and then the catalyst was illuminated by two 8 W UV-lamps with the optimal wavelength of 365 nm. The main oxidation products were CO_2 and H_2O and only a small amount of acetaldehyde was produced during reaction. Unreacted hexane was analyzed by a gas chromatograph equipped with a flame ionization detector (FID). The photocatalytic activity of the catalysts reached steady state after about 6 h and all the activity data referred in this work were obtained at steady state. The photocatalytic oxidation of methanol (1100 ppm) was carried out in the same fix-bed flow reactor under similar reaction conditions.

3. Results

3.1. Characterization of nanosized zirconia

In order to obtain the zirconia catalysts with different forms, the prepared zirconia precursor was calcined at various temperatures, their XRD patterns are shown in Fig. 1. The crystalline phase of these calcined catalysts are different. All of the catalysts are amorphous after calcination at

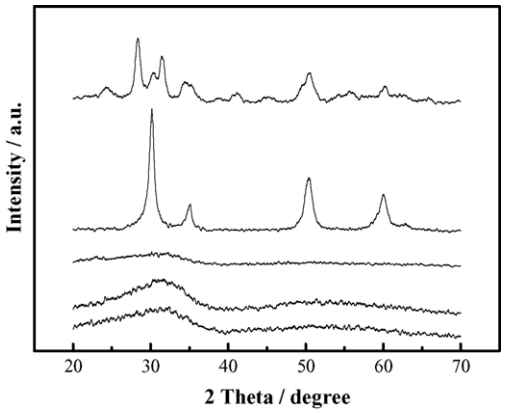

Fig. 1. XRD patterns of zirconia samples. From bottom to top: ZrO_2-0-110, ZrO_2-0-110-200, ZrO_2-0-110-300, ZrO_2-0-110-450 and ZrO_2-110-650.

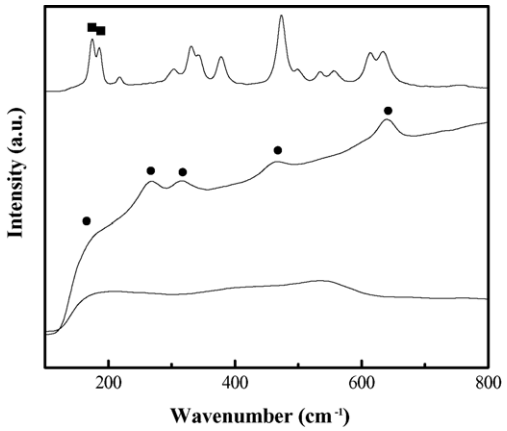

Fig. 2. Raman spectra of zirconia samples. From bottom to top: ZrO_2-0-110, ZrO_2-0-110-450, ZrO_2-110-650; (●) tetragonal; (■) monoclinic.

a temperature below 300 °C. When the temperature reaches 450 °C, the peaks at 29.8°, 34.2°, 49.6° and 59.5° appears, corresponding to the diffractions of (1 0 1), (0 0 2), (1 1 2) and (2 1 1) of tetragonal ZrO_2, respectively, indicating zirconia catalyst with pure tetragonal phase is obtained. These results are in good agreement with previous literature [11,12], which reported that the phase transformation of zirconia from amorphous to tetragonal form takes place at about 400 °C. A mixture of monoclinic and tetragonal zirconia catalyst, predominantly in monoclinic phase was obtained by the hydrolysis of $Zr(OC_3H_7)_4$. The peaks at 24.0°, 28.2°, 31.5°, 41.0°, 45.0° and 55.8° are the diffraction of (0 1 1), (1 1 $\bar{1}$), (1 1 1), (2 1 $\bar{1}$), (1 1 2) and (1 3 0) of monoclinic ZrO_2, respectively.

Raman spectroscopy was applied in the present investigation because of its sensitivity in determining the local order, so as to compensate for XRD shortcomings dealing with short-range structures. Fig. 2 shows the Raman spectra of three representative zirconia samples. According to previous Raman studies, ZrO_2 in tetragonal form has six Raman active modes and is identified by peaks at 148 and 263 cm^{-1}, whereas monoclinic ZrO_2 has 18 Raman active modes with diagnostic twin-peaks at 170–180 and 180–190 cm^{-1} [13–15]. In the Raman spectrum of ZrO_2-0-110-450, the peaks at 150, 264, 321, 464 and 640 cm^{-1} are observed, characteristic of tetragonal phases of zirconia. For ZrO_2-110-650, multiple Raman peaks assignable to monoclinic zirconia are found. Only several weak bands are present in the Raman spectrum of ZrO_2-0-110, which could be assigned to the bending and stretching of zirconium–oxygen bond, indicating its amorphous structure. These results agree quite well with the XRD measurements.

The specific surface areas of the prepared catalysts were measured by N_2 adsorption methods and listed in Table 1. The surface area of the catalysts decreased gradually with the increased calcination temperature. Moreover, the surface area of monoclinic catalyst is much lower, only one-third of that of tetragonal one.

TEM micrographs of some of the representative catalysts are shown in Fig. 3. In the ZrO_2-0-110 samples, no clear particles can be observed and all are adhere to each other, forming hard agglomerates. The ZrO_2-0-110-450 sample consists of irregular spherical grains and the grain sizes are in the range of 15–30 nm. The ZrO_2-110-650 sample has the similar morphology, but its gain sizes are about 30–50 nm, relatively larger compared with ZrO_2-0-110-450.

Table 1
Textural properties and activities of various photocatalysts

Sample	Surface area ($m^2\ g^{-1}$)	Conversion of hexane (%)[a]	Conversion of methanol (%)[a]
ZrO_2-0-110	289	25.6	31.6
ZrO_2-0-110-200	248	22.1	27.2
ZrO_2-0-110-300	181	2.9	10.2
ZrO_2-0-110-450	121	3.7	15.4
ZrO_2-110-650	34	4.5	12.3
ZrO_2-0-110/SO_4^{2-}-110	168	0	9.7
ZrO_2-0-110/SO_4^{2-}-650	82	0	5.6
P25	48	17.3	40.3

[a] 7 h after illuminated by UV-lamps with the optimal wavelength of 365 nm.

UV–vis diffuse reflectance spectra of representative samples, ZrO_2-0-110, ZrO_2-0-110-450 and ZrO_2-110-650 are shown in Fig. 4. For all the samples, a non-negligible absorption in the near-UV range of 290–390 nm is observed, which agrees with previous reports [3,4]. Crystallization of amorphous samples on calcinations induces a red shift of the absorption edge [8]. The spectra of three samples are similar in the absorption peak shape and strength, indicating their similar photoabsorbed properties despite of their different phase structure.

3.2. Photocatalytic activity of various zirconia samples

Using gas-phase photo-oxidation of hexane and methanol as probe reactions, the photocatalytic activity of various forms of zirconia was tested under the illumination of two UV-lamps with the optimal wavelength of 365 nm. The steady state conversions of hexane and methanol are given in Table 1, together with Degussa P25 for comparison. The activities of crystalline zirconia catalysts, either tetragonal or monoclinic, are quite low, while the amorphous catalysts prepared by calcining at 100 and 200 °C are very active. Their activities of hexane oxidation reach 25.6 and 22.1%, respectively, which are even higher than that of Degussa P25 (17.3%). The zirconia catalyst prepared by calcination at 300 °C has a very low activity, though it retains amorphous structure and comparable surface area. To explain such an unexpected result, thermal gravimetric analysis of ZrO_2-0-110, ZrO_2-0-110-200, ZrO_2-0-110-300 and ZrO_2-0-110-450 was carried out in flowing N_2. The DTG/DTA profiles of the samples are shown in Fig. 5. Two endothermic peaks are observed on the DTG profiles of ZrO_2-0-110 and ZrO_2-0-110-200, which are associated with the desorption of physically adsorbed water and the dehydroxylation of surface hydroxyls on ZrO_2. But only peaks around 88 °C are observed on the DTG profiles of ZrO_2-0-110-300 and ZrO_2-0-110-450, indicating that there

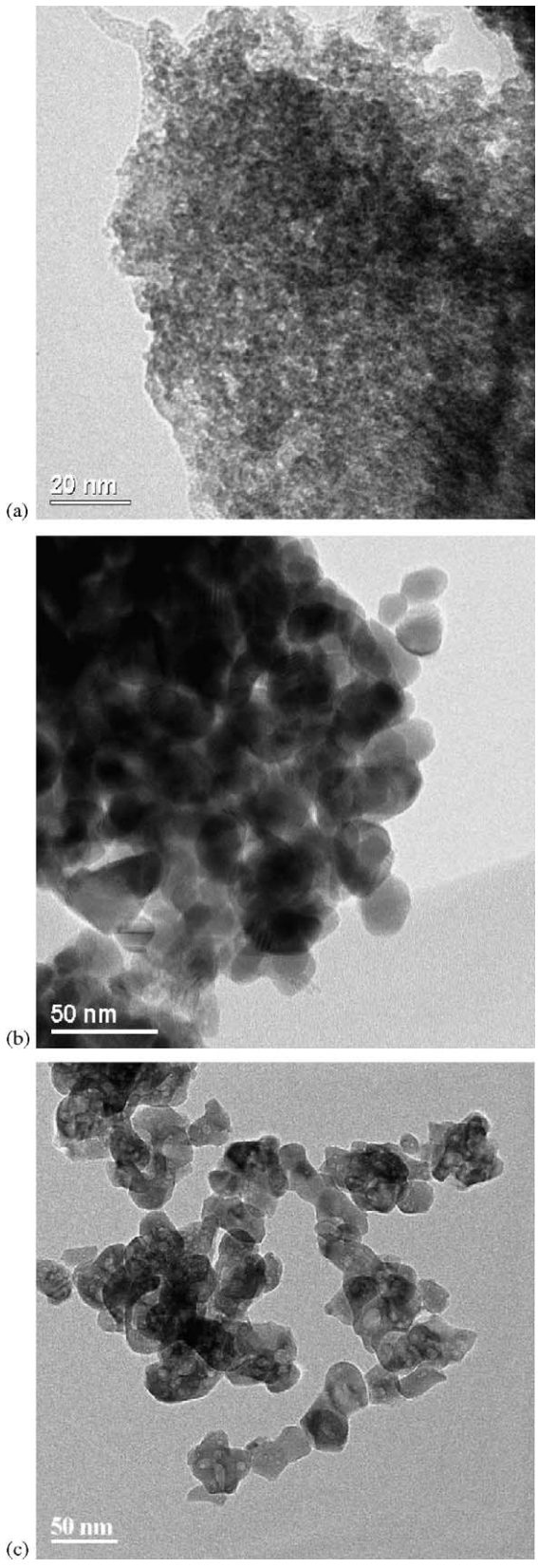

Fig. 3. TEM micrographs of the samples: (a) ZrO_2-0-110; (b) ZrO_2-0-110-450; (c) ZrO_2-110-650.

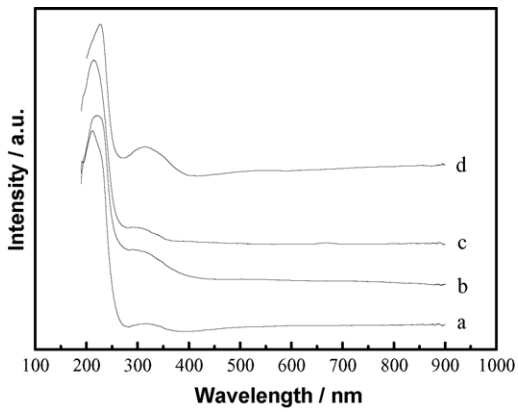

Fig. 4. UV–vis diffuse reflectance spectra of various zirconia samples: (a) ZrO_2-0-110/SO_4^{2-}-650; (b) ZrO_2-0-110-450; (c) ZrO_2-0-110; (d) ZrO_2-110-650.

are little surface hydroxyls left on these catalysts after calcinations at relative high temperature. The existence of surface hydroxyls is probably the cause for the high photocatalytic activities of ZrO_2-0-110 and ZrO_2-0-110-200.

In the UV–vis diffuse reflectance spectra, ZrO_2-0-110 and ZrO_2-0-110-450 show a maximum absorption around 250 nm. Since the photocatalytic performance of the catalyst is related to the wavelength of illumination light [16,17],

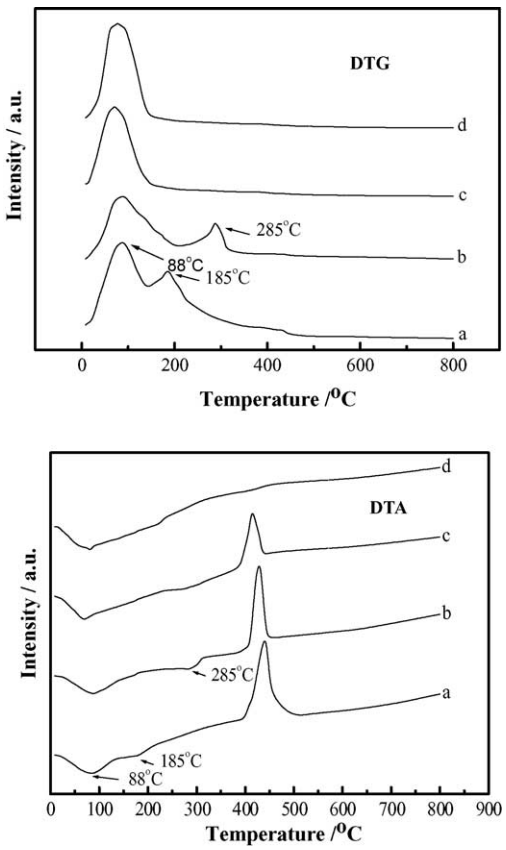

Fig. 5. Thermograms of various zirconia samples: (a) ZrO_2-0-110; (b) ZrO_2-0-110-200; (c) ZrO_2-0-110-300; (d) ZrO_2-0-110-450.

Table 2
Activities of various zirconia samples illuminated by UV-lamps with different optimal wavelengths

Sample	Conversion of hexane (%)	
	I	II
ZrO_2-0-110	25.6	29.4
ZrO_2-0-110-450	3.7	9.3
ZrO_2-110-650	4.5	9.7

I: 7 h after illuminated by UV-lamps with the optimal wavelength of 365 nm; II: 7 h after illuminated by UV-lamps with the optimal wavelength of 253.7 nm.

UV-lamps with the optimal wavelength of 253.7 nm matching the band gap energy of these samples was used. The activities of various samples under such lamps are shown in Table 2. Obviously, the photocatalytic activities of these samples are improved under illumination light with suitable wavelength. Among the three catalysts tested, amorphous zirconia calcined at 110 °C exhibits highest activity, just as above.

3.3. Effect of sulfation on the photoactivity of ZrO_2

Sulfated zirconia catalysts were prepared by immersing the ZrO_2-0-110 sample in 1 mol l^{-1} H_2SO_4 and then drying at 110 °C. The XRD patterns of the sulfated catalysts before and after calcined at 650 °C are shown in Fig. 6. The structure of the sulfated catalyst before calcination retains amorphous. After calcination at 650 °C, the catalyst shows a mixture of monoclinic and tetragonal structure, in which tetragonal is the main phase. The surface area of the sulfated catalysts measured by N_2 adsorption is listed in Table 1. The ZrO_2-0-110/SO_4^{2-}-110 sample has much smaller specific surface area after sulfation, and moreover, the surface area is reduced further to 82 m^2 g^{-1} after calcination at 650 °C.

The photocatalytic activities of the sulfated catalysts on the photo-oxidation of hexane and methanol were tested and the results are listed in Table 1 as well. The activities reduced dramatically after sulfation, the conversion of hexane and methanol over ZrO_2-0-110/SO_4^{2-}-110 are much lower than that of ZrO_2-0-110, and the activities decrease further after calcination at 650 °C due to the decreasing of the surface area. Sulfation renders a negative effect on the photocatalytic activity of zirconia catalysts.

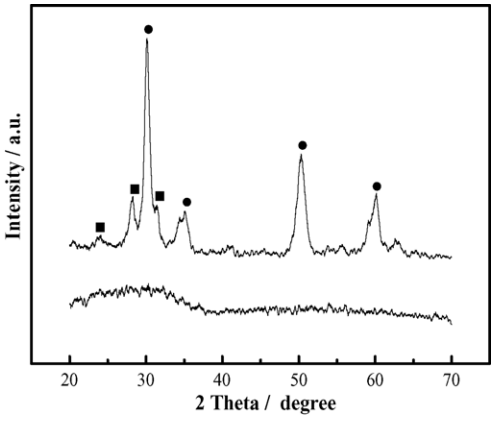

Fig. 6. XRD patterns of sulfated zirconia samples. From bottom to top: ZrO_2-0-110/SO_4^{2-}-110, ZrO_2-0-110/SO_4^{2-}-650; (●) tetragonal; (■) monoclinic.

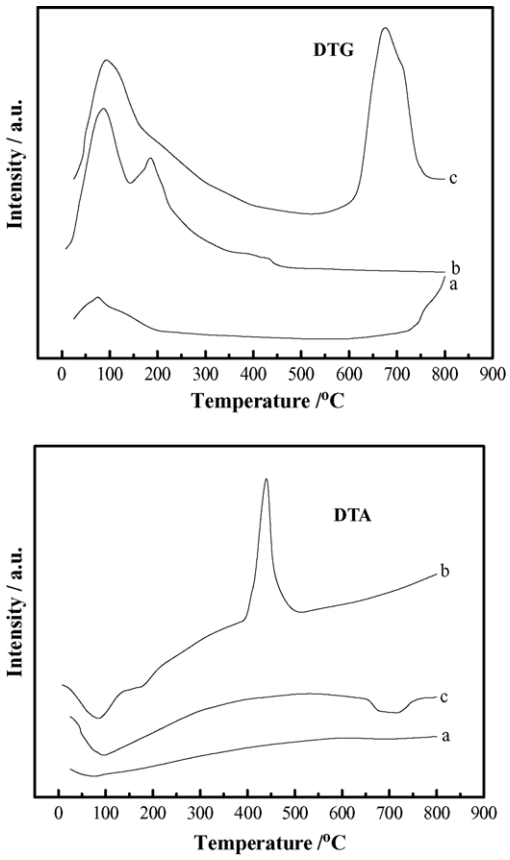

Fig. 7. Thermograms of sulfated zirconia samples: (a) ZrO_2-0-110/SO_4^{2-}-650; (b) ZrO_2-0-110; (c) ZrO_2-0-110/SO_4^{2-}-110.

Thermal gravimetric analysis was again employed to explain this negative effect. Fig. 7 depicts the DTG/DTA profiles of sulfated catalysts. Only one endothermic weight loss peak centered at 80 °C was observed on both sulfated catalysts, corresponding to the desorption of physically adsorbed water. In the meantime, an extra exothermic peak around 700 °C is observed, corresponding to the release of SO_3. No evident peak of the dehydroxylation of surface hydroxyls is observed for both of the sulfated samples, which probably account for their low photocatalytic activity. The details of this phenomenon deserve further studies.

UV–vis diffuse reflectance spectrum of ZrO_2-0-110/SO_4^{2-}-650 is shown in Fig. 4. As compared with zirconia with amorphous or pure tetragonal phase, ZrO_2-0-110/SO_4^{2-}-650 calcined at a higher temperature induces a red shift of the absorption edge probably due to grain growth. However, the absorption spectrum is similar in peak shape and strength as non-sulfated sample, which indicates that sulfation has no significant effect on the photoabsorbed properties of the sample.

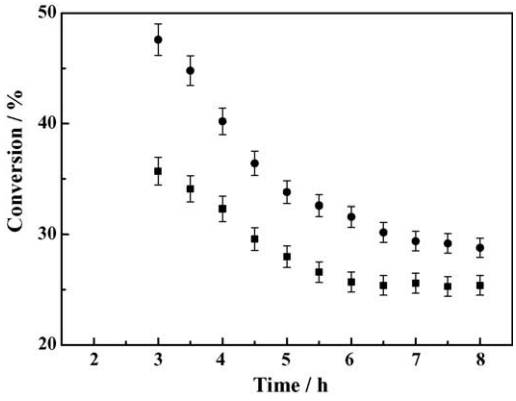

Fig. 8. Activity of hexane oxidation over ZrO_2-0-110 as a function of reaction time. Reactant: 1700 ppm hexane in air; catalyst: 0.3 g ZrO_2-0-110; GHSV: 4000 h^{-1}; (●) UV-lamps with wavelength of 253.7 nm; (■) UV-lamps with wavelength of 365 nm.

3.4. Stability of the catalysts

The conversion of hexane and methanol over ZrO_2-0-110 catalysts as a function of reaction time was studied and depicted in Figs. 8 and 9. For all the reactions, the conversion drops gradually in the initial reaction period and reaches steady state after about 7 h, which is just the same as that over titania catalysts [18]. According to previous studies [19], the adsorption of less reactive partial oxidation intermediates on the catalyst surface may be responsible for the initial deactivation.

The photocatalytic oxidation reaction of hexane has been run continuously on ZrO_2-0-110 catalyst for 100 h, which showed a maximum catalytic activity in the reaction, and the results are shown in Fig. 10. It can be seen that the catalyst was rather stable after the initial deactivation. The steady-state conversion of hexane during the reaction is about 23%, higher that of standard photocatalyst Degussa P25. The long-term test results show that amorphous zirconia samples prepared in this experiment possess both rather high photoactivity and stability, which predict them to be a potential practical photocatalyst.

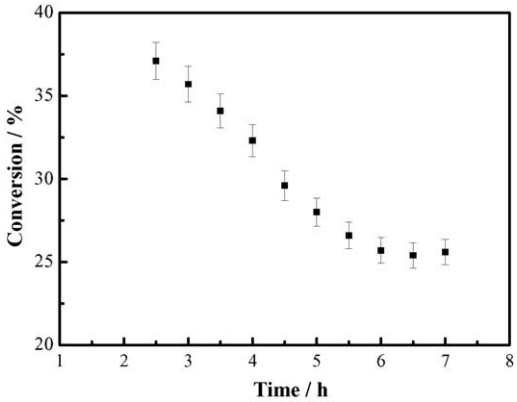

Fig. 9. Activity of methanol oxidation over ZrO_2-0-110 as a function of reaction time. Reactant: 1100 ppm methanol in air; catalyst: 0.3 g ZrO_2-0-110; GHSV: 4000 h^{-1}; UV-lamps with wavelength of 365 nm.

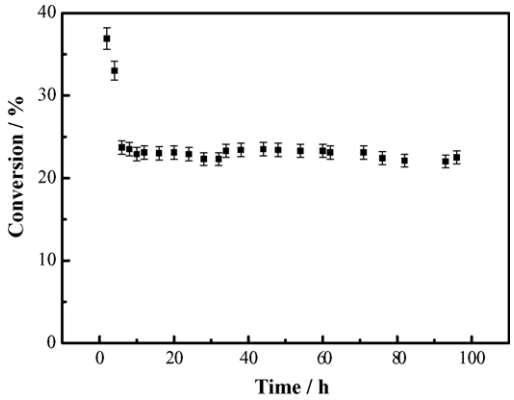

Fig. 10. Long-term test results of ZrO_2-0-110 illuminated by UV-lamps with the optimal wavelength of 365 nm. Reactant: 1700 ppm hexane in air; catalyst: 0.3 g; GHSV: 4000 h^{-1}.

4. Discussion

The valence band electrons of ZrO_2 can be excited to the conduction band under illumination of ultraviolet light, and highly reactive electron–hole pairs are produced. The electrons and holes after migration to the catalyst surface are capable of reducing and oxidizing surface-adsorbed substrates in the gas-phase photo-oxidation. Furthermore, the positive hole can also react with surface hydroxyl to form OH radical, whereas the electron is trapped by surface-adsorbed oxygen to form superoxide:

$$ZrO_2 + h\nu \leftrightarrows e^- + h^+$$

$$e^- + O_2 \rightarrow O_2^-$$

$$h^+ + S \rightarrow S_{ox}^+$$

$$h^+ + OH^- \rightarrow OH$$

where e^- is an electron and h^+ is a positive hole, and S and S_{ox}^+ are the adsorbed organic substrate and its oxidized product, respectively. The OH radical and superoxide are both effective oxygenation agents, which are able to degrade a great variety of organic compounds [1,18].

Since the photocatalytic oxidation reactions via interfacial charge transfer between the surface-adsorbed species, reduction in the surface recombination of electron–hole pair lead to a high efficiency of the photocatalytic process. Some researchers [8,20] claim that high crystallinity, decreasing defects acting as the electron–hole recombination center, improve photocatalytic activity of TiO_2 catalysts. In contrast to the general results for TiO_2, amorphous but not crystalline ZrO_2 catalysts show the higher activity. This high photo-activity may be due to the abundance of hydroxyl groups present on the catalyst surface, which can prevent

the electron–hole recombination by trapping hole and generating OH radicals acting as powerful oxidants. This has been proved by the thermal gravimetric experiments shown in Fig. 5. Similar results were observed for the Nb_2O_5 photocatalyst by Kominami et al. [8].

It was reported that sulfation of anatase titania enhances its activity for photocatalytic oxidation of CH_3Br, C_6H_6 and C_2H_4. The improved activity for the sulfated titania catalysts is not only due to a greater surface area but also the increased surface acidity [18]. It is well known that sulfation of amorphous ZrO_2 will create strong acid sites on the surface, which have high catalytic activity for the conversion of small hydrocarbon at low temperature [21]. But sulfation does not improve the photo-catalytic activity of ZrO_2 catalysts in the gas-phase oxidation of hexane or methanol as expected. On the contrary, the activities reduced dramatically after sulfation. This negative effect can also be explained by the decreasing of the hydroxyl group on the surface, which may be caused by the reaction between the hydroxyl group and the sulfate group. The result indicates that the hydroxyl groups not the acid sites play an important role in the ZrO_2 photo-catalytic reactions.

5. Conclusion

Nanosized zirconia with different phase structure and surface area were prepared and characterized. The effect of the phase structure, specific surface area and the surface property on the photocatalytic activity of ZrO_2 catalysts was studied systematically. The amorphous ZrO_2 prepared below 200 °C in this experiment shows much higher activity than that of the crystalline samples for the gas-phase photocatalytic oxidations of hexane and methanol, presumably due to the abundance of the hydroxyl groups on the catalyst surface. Sulfation of the ZrO_2 results in a decrease in the amount of surface hydroxyl groups of the catalysts, leading to a negative effect on the photocatalytic activity of the catalysts. The results of a long-term test of 100 h show that the activity of the amorphous zirconia photocatalysts is very stable.

Acknowledgements

This work was supported by the Chinese Major State Basic Research Development Program (grant no. 2000077507), the National Natural Science Foundation of China (grant no. 20303004) and the Shanghai Major Basic Research Program (grant no. 03DJ14004).

References

[1] M.R. Hoffmann, S.T. Martin, W. Choi, D.W. Bahnemann, Chem. Rev. 95 (1995) 69.
[2] K.M. Ganguly, S. Sarkar, S.N. Bhattacharyya, J. Chem. Soc., Chem. Commun. (1993) 682.
[3] S.G. Botta, J.A. Navía, M.C. Hidalgo, G.M. Restrepo, M.I. Litter, J. Photochem. Photobiol. A: Chem. 129 (1999) 89.
[4] J.A. Navio, M.C. Hidalgo, G. Colón, S.G. Botta, M.I. Litter, Langmuir 17 (2001) 202.
[5] S. Sato, T. Kadowaki, J. Catal. 106 (1987) 295.
[6] K. Sayama, H. Arakawa, J. Phys. Chem. 97 (1993) 531.
[7] Y. Kohno, T. Tanaka, T. Funabiki, S. Yoshida, J. Chem. Soc., Faraday Trans. 94 (1998) 1875.
[8] H. Kominami, K. Oki, M. Kohno, S. Onoue, Y. Kera, B. Ohtani, J. Mater. Chem. 11 (2001) 604.
[9] Y.H. Yue, X.P. Zhao, W.M. Hua, Z. Gao, Appl. Catal. B 46 (2003) 561.
[10] H. Nakabayashi, Chem. Lett. (11) (1996) 945.
[11] X. Bokhimi, A. Morales, O. Novaro, M. Portilla, T. López, F. Tzompantzi, R. Gómez, J. Solid State Chem. 135 (1998) 28.
[12] T. Sato, J. Therm. Anal. Calc. 69 (2002) 255–265.
[13] E. Djurado, P. Bouvier, G. Lucazeau, J. Solid State Chem. 149 (2000) 399.
[14] Sekuli, K. Furi, M. Stubiar, J. Mol. Struct. 410–411 (1997) 275.
[15] P. Barberis, T. Merle-Méjean, P. Quintard, J. Nucl. Mater. 246 (1997) 232.
[16] V. Emeline, A.V. Rudakova, V.K. Ryabchuk, N. Serpone, J. Phys. Chem. B 102 (1998) 10906.
[17] V. Emeline, G.N. Kuzmin, D. Purevdorj, V.K. Ryabchuk, N. Serpone, J. Phys. Chem. B 104 (2000) 2989.
[18] X.Y. Deng, Y.H. Yue, Z. Gao, Appl. Catal. B 39 (2002) 135.
[19] M.C. Blount, J.L. Falconer, J. Catal. 200 (2001) 21.
[20] K. Nagaveni, G. Sivalingam, M.S. Hegde, G. Madras, Appl. Catal. B 48 (2004) 83.
[21] S. Raz, K. Sasaki, J. Maier, I. Riess, Solid State Ionics 143 (2001) 181.